



Ordinal patterns-based methodologies for distinguishing chaos from noise in discrete time series

Massimiliano Zanin ^{1,2}✉ & Felipe Olivares ^{1,2}

One of the most important aspects of time series is their degree of stochasticity vs. chaoticity. Since the discovery of chaotic maps, many algorithms have been proposed to discriminate between these two alternatives and assess their prevalence in real-world time series. Approaches based on the combination of “permutation patterns” with different metrics provide a more complete picture of a time series’ nature, and are especially useful to tackle pathological chaotic maps. Here, we provide a review of such approaches, their theoretical foundations, and their application to discrete time series and real-world problems. We compare their performance using a set of representative noisy chaotic maps, evaluate their applicability through their respective computational cost, and discuss their limitations.

One of the challenges underpinning the study of many real-world systems is that the mechanisms governing their behaviour are not easily accessible and can only indirectly be observed through their visible dynamics; making a parallelism with genetics, the phenotype should be used to infer the genotype. One of the most basic questions that can be made is whether observed time series are generated by stochastic processes or are instead the result of a deterministic dynamics. In the latter case, models can be used to forecast the evolution of the system with an arbitrary precision, something not possible for a stochastic process, and ultimately, to completely describe the system under study. On the other hand, a stochastic dynamics may indicate that the observable under study is not the most appropriate one. Answering to such question can nevertheless be a daunting task. First of all, the extracted time series are usually a combination of both aspects, i.e. the observations we perform on a system are most probably polluted by some kind of observational or systemic noise. Second, real-world systems can only be described by finite, and usually short, time series: the answer may then vary according to the used methods and parameters^{1–3}. Third, it is long known that some deterministic systems produce time series that are (almost) indistinguishable from noise: chaotic systems. Chaotic systems can be defined as a class of dynamical systems displaying three properties: sensitivity to initial conditions, topologically transitivity, and presence of dense periodic orbits⁴. Finally, noise and chaos are two intermingled concepts, as for instance the former can induce the latter⁵.

Given a time series, determining its stochastic or deterministic nature is *in theory* simple and involves measuring two quantities. On one hand, the maximum Lyapunov exponent (λ), describing the sensitivity to initial conditions; and the Kolmogorov–Sinai entropy per unit time (h_{KS}) on the other hand, i.e. the amount of information the system is generating. Yet, these two measures can only be calculated in infinitely long time series; the answer is thus not readily available for real, and hence finite, observations. Not surprisingly, many other methods have been proposed, e.g. based on finite-size Lyapunov exponents⁶, power spectra⁷, non-linear forecasts^{8–10}, recurrence networks^{11,12} or visibility graphs^{13,14}.

¹Instituto de Física Interdisciplinar y Sistemas Complejos CSIC-UIB, Edifici Instituts Universitaris de Recerca, Palma de Mallorca, Spain. ²These authors contributed equally: Massimiliano Zanin, Felipe Olivares. ✉email: massimiliano.zanin@gmail.com

A promising approach is the one yielded by the concept of *permutation patterns*, introduced in 2002 by Bandt and Pompe¹⁵. Given a time series x_t , this is partitioned in (usually, but not always, overlapping) subsets of consecutive values ($x_t, x_{t+\tau}, \dots, x_{t+\tau(d-1)}$); d , i.e. the number of values composing each subset, is called the *embedding dimension*, and is usually set between 3 and 7; and τ is the *embedding delay*, or the time between consecutive points, usually set to 1. A *permutation pattern* (also called *order* and *ordinal* pattern interchangeably in the literature) π_t is then associated with each subset, i.e. the permutation that has to be applied to the subset to obtain an increasing set of values—see Fig. 1a. Once this process is repeated for all subsets of values, statistics can be calculated over the resulting permutation pattern distribution, to obtain e.g. entropies^{15–17} or irreversibility^{18–20}, or to discriminate the nature of the underlying systems^{21–25}. When compared to other time series metrics, this approach has several major advantages: it is almost parameter-free, in that symbols (i.e. the permutation patterns) naturally emerge from the time series; it has low sensitivity to noise and is invariant under monotonic transformations of the values; is computationally inexpensive; and, possibly the most important point, naturally takes into account the causal order of elements. The interested reader will find several reviews on the concept of permutation entropy^{26–28}, and many works discussing specific aspects of it^{29–34}, as e.g. the choice of the best embedding dimension.

Given the success of permutation patterns and permutation entropy in characterising time series, a natural question is whether they can be used to assess their chaotic or stochastic nature. Many approaches leveraging on this idea have been proposed, both using variants of the permutation entropy alone and by combining it with other time series metrics. In this review, we provide an in-depth analysis of the theoretical foundations and the applicability of such methods to time-discrete systems, organised into three categories: individual metrics based on the permutation patterns idea; combination of metrics yielding plane representations; and pipelines, i.e. decision trees like algorithms³⁵. These metrics are then compared using a set of synthetic time series, to assess both their discriminative performance and their computational cost. We further discuss some preliminaries on the use of such metrics, including their applicability to continuous systems, and their associated theoretical limits. This review will therefore serve as a guide, both to the practitioner new to this topic who wants to analyse real-world time series and to the experienced researcher looking for new venues of investigation.

Some preliminary practical considerations on evaluating permutation patterns

Before digging into the study of the individual algorithms based on permutation patterns, we here discuss three preliminary issues that can cause problems to the researcher new to this topic. Note

that we suppose the reader to already be familiar with the concept of permutation entropy; otherwise, we invite him/her to refer to several comprehensive reviews available in the literature^{26–28}.

- *Labelling of permutation patterns.* There are two ways of naming permutation patterns, which have vastly been used in the literature in an interchangeable way. Let us consider the case of the pattern associated with values $x = \{8, 3, 6\}$. On one hand, this pattern may be defined as the sequence of ranking positions of the individual elements, in ascending order; the first element of the ranking would then be 3, followed by 6 and 8. Substituting the values by the respective ranking, one gets $\pi = (3, 1, 2)$. On the other hand, the pattern can be created by combining the indexes of the elements giving the correct ascending order. In the previous example, the smallest element is the second, followed by the third and the first; the resulting pattern is then $\pi = (2, 3, 1)$. This difference in labelling does not affect any result, as what is important is the relative frequency of patterns.
- *Naming convention.* Parameters used in the calculation of permutation patterns and the corresponding results have been denoted by different symbols in the literature—see Fig. 1b for a list of the most common variants. Special attention should be paid in those case in which the same symbol represents two different things, as e.g. L being both the embedding delay³⁶ and dimension³⁷.
- *Equal values in the time series.* When analysing real-world time series, it is not uncommon to find equal values, something especially frequent when dealing with low-resolution time series, as e.g. weak biological signals. Note that this is not compatible with the previous definition of permutation patterns, which requires values to be uniquely sorted. The two main solutions were already proposed in the original paper of Bandt and Pompe¹⁵. First, one can disregard equal values by e.g. converting the inequality $x_1 < x_2 < x_3$ to $x_1 \leq x_2 \leq x_3$; second, one can numerically break equalities by adding small random perturbations, e.g. a normally distributed noise of low amplitude. A third solution entails mapping the equal values onto the same symbols³⁸; to illustrate, the time series $x = \{6, 6, 82\}$ is transformed in the permutation pattern $\pi = (1, 1, 3)$. However, this latter strategy does not lead to a uniform distribution for a totally random sequence, i.e. for white noise. The impact of equal values is still a matter of debate in the scientific community. It has been shown that spurious temporal correlations can not only be introduced by repeated values³¹ but also that they have a small or even negligible impact in real-world time series with a decent resolution³⁴. In any case, the reader should be aware of this limitation and eventually pre-process the data accordingly.

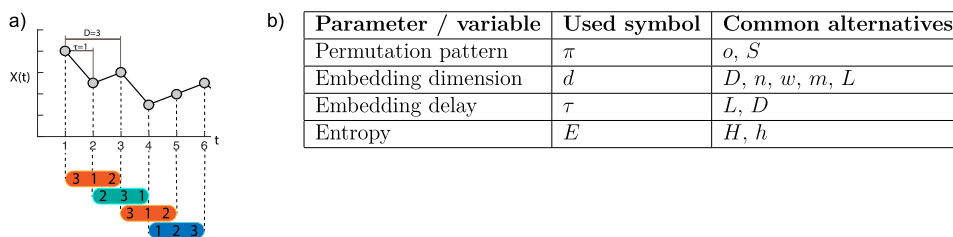


Fig. 1 Mapping time series to ordinal patterns. **a** Example to illustrate the methodology of mapping a time series into a set of overlapped ordinal patterns, for an embedding dimension $d = 3$ and an embedding delay $\tau = 1$. Each pattern is obtained by substituting the original values by the respective ranking. For instance, the second value is the smallest of the first three and is thus mapped to number 1 in the first pattern. Note that different symbols have been used to denote the main parameters used in permutation patterns analysis; **b** reports the symbols used in this work and common variants in the literature.

Finally, as previously introduced, this review is mainly focussed on the analysis of time-discrete systems. Still, the methods here presented have been the foundation for extensions covering irregularly sampled and continuous time series. Regarding the former case, Kulp et al.³⁹ analysed for the first time irregularly sampled time series, i.e. when data are missing or a time jitter is present. In both cases, a low degree of irregularity does not prevent missing patterns (introduced in section “Individual metrics”) to detect determinism. The interested reader can also explore subsequent works^{40,41}. On the other hand, several studies have focussed on continuous systems^{39,42–45} and on continuous systems with delay^{46,47}. The reader should nevertheless be aware that (at times, hidden) assumptions of these approaches is that the sampling frequency is the correct one to describe the underlying dynamics, something which can be estimated using classical tools like the Nyquist frequency, and that the embedding delay τ is fixed to one, even though multi-scale analyses are possible and beneficial^{48,49}.

Individual metrics

Missing ordinal patterns. The first proposal for a metric able to discriminate stochastic from deterministic dynamics using permutation patterns and entropy was formulated back in 2006 by Amigó and co-workers⁵⁰. They started from realising that, while some chaotic maps are able to produce time series much resembling random noise, at the same time they cannot reproduce all ordinal patterns. To illustrate, consider the case of the well-known logistic map $f(x) = 4x(1 - x)$; it is easy to show that the pattern $\pi = (2, 1, 0)$ can never appear, as well as the general pattern $\pi = (*, 2, *, 1, *, 0, *)$ (where $*$ denotes any other ranking position), as the succession $f^2(x) < f(x) < x$ can never occur. This, in turns, triggers an avalanche of longer *forbidden* patterns, which also cannot occur⁵⁰. Given one time series, one can then suspect the presence of a deterministic dynamics if at least one permutation pattern never shows up.

This approach nevertheless presents a caveat: when analysing short time series, i.e. in many real applications, patterns may be missing just because of a statistical effect, i.e. not enough dynamics has been observed to allow all patterns to emerge. These are the so-called *false* missing patterns. Amigó et al.⁵¹ showed that the minimum time series length to avoid such effect is $(d + 1)!$, with d being the length of the patterns. Alternatively, one can analyse how the number of forbidden patterns decays as a function of the time series length, being such decay faster in deterministic maps⁵¹.

A more quantitative statistical test was subsequently proposed by the same authors⁵². Suppose a time series on which permutation patterns of size d are extracted using sliding windows overlapping at a single point (i.e. the last point of a window is the first point of the next one). The total number of resulting subwindows is denoted by K . Next, one counts the number of times a specific permutation pattern i is observed and denotes it as ν_i , with $i = \{1, 2, \dots, d!\}$. The deterministic nature of the time series can be tested through a χ^2 test with statistic:

$$\chi^2 = \sum_{j=1}^{d!} \frac{(\nu_j - K/d!)^2}{K/d!}. \quad (1)$$

In other words, the aim is to compare the observed distribution of pattern frequencies with the one expected in a completely random time series—which, by definition, is uniform. The advantage of this test is that not only it detects cases of missing permutation patterns but also situations in which their relative frequency is unbalanced.

Going back to the concept of missing patterns, an additional method based on it was proposed in 2019 by Olivares and co-workers⁴⁵. This method is first based on dividing the original time series into sliding, nonoverlapping windows of size w . The number of unobserved (i.e. missing) ordinal patterns is then counted within each one of these windows, and the average number $\langle N(w, d) \rangle$ is calculated—note that this number is given as a function of w and of the embedding dimension d . Finally, the decay of the missing patterns is modelled with a stretched exponential function:

$$\langle N(w, d) \rangle = Ae^{-Bw^\gamma}, \quad (2)$$

where A is a constant, B is the characteristic decay rate and γ is the stretching exponent. The estimated B and γ can then be used to classify the time series; specifically, stochastic time series are characterised by $B < 10^{-2}$ and $\gamma > 0.6$ when using $d = 6$, while chaotic systems (even polluted by additive noise) have larger values of B and smaller values of γ .

Being the concept of missing or infrequent ordinal patterns the foundation of all methods here presented, a review of all real-world applications would exceed the scope of the present work. The interested reader can nevertheless refer to the many reviews on the topic^{26–28,53,54}.

Permutation spectrum test. Kulp and Zunino proposed in 2014 a method that can be seen as an evolution of what previously described, and which is based on the idea of the permutation spectrum test. If the method of Amigó et al.⁵² was based on reconstructing and studying the shape of the probability distribution created by permutation patterns, Kulp and Zunino⁵⁵ shift the focus to the variability of such distribution.

As usual, let us suppose a time series, which is here divided in non-overlapping windows of length l . The probability distribution of permutation patterns, here called *spectrum*⁵⁵, is then calculated, i.e. how many times each pattern appears in each window. Finally, the standard deviation of the probability associated with each pattern is calculated. The key to distinguish between different types of dynamics resides in those standard deviations. For instance, all patterns will have no variability at all (i.e. a standard deviation of zero) for periodic signals—as the same permutations will appear over and over without any variation. Conversely, stochastic time series will be characterised by a positive variability for all permutation patterns. Finally, chaotic signals will lie in the middle, with some patterns (i.e. the forbidden ones) having zero standard deviation.

This approach has a remarkable advantage: by studying subwindows of the original time series, it is able to detect intermittent dynamics, provided a suitable value of l is chosen. On the other hand, all patterns have to appear, and l must be large enough—using the standard rule proposed by Amigó et al.⁵¹, $l \gg (d + 1)!$, with d being the embedding dimension; hence, the time series should globally be much larger than l , in order to have enough values for the calculation of the standard deviation. All in all, this could be a problem in real-world applications, where the length of the time series is limited.

The permutation spectrum test has been applied to several real-world time series, including the pressure signal acquired from a turbulent combustor with bluff-body and swirler as flame holding devices⁵⁶, measures of flame fronts in a lean swirling premixed flame generated by a change in gravitational orientation⁵⁷ and ocean ambient noise⁵⁸.

Complementing permutation entropy with cylinder sets. One theoretically simple way of discriminating chaotic from stochastic processes is by calculating their KS entropy h_{KS} , which represents

the entropy required to characterise the evolution of trajectories⁵⁹. In other words, and given an initial value x_0 , h_{KS} tells us how the precision of our prediction for value x_n decreases with n . As such, it has been proven that there is a relationship between h_{KS} and the Lyapunov exponents of the system⁶⁰. A test is then easy to define: $h_{KS} = 0$ for stable systems; chaotic systems are characterised by finite (positive) Lyapunov exponents, and hence finite (yet, greater than zero) h_{KS} ; finally, for stochastic systems, as the future cannot be forecasted at all, h_{KS} diverges to infinity. This is nevertheless not simple from an applied point of view, as the computation of h_{KS} can only be done in an approximate way⁶¹. A solution may come from the permutation entropy. Specifically, it has been shown that e_p is equal to h_{KS} for one-dimensional (1D) and 1D-like maps^{62,63}. Note that here e_p is the time derivative of the permutation entropy, i.e. $e_p = [E_p(d+1) - E_p(d)]/T$, d being the embedding dimension and T the time resolution (or the length of the time steps) of the series. Yet, what about more complex chaotic systems?

Politi proposed an elegant solution⁶⁴. First of all, he defines $\sigma_i(j)$ as the dispersion of $x_i(j)$ (with $1 \leq j \leq d$), i.e. of all the values in the j th position of the i th ordinal pattern. $\sigma_i(j)$ thus tells us how much uncertainty we have about the value of the time series, if we know that such value appears in the j th position of the i th ordinal pattern. As the system evolves over time, the largest value of $\sigma_i(j)$ will always be found for $j = d$, and hence the important value is $\sigma_i(d)$. This value is then used to define a relative permutation entropy, as $\tilde{E}_p(d) = E_p(d) + D(\log(\sigma_i(d)))$. Note that $\langle \cdot \rangle$ denotes the average, while D is the fractal (information) dimension of the system. Finally, he demonstrates that $\tilde{e}_p(d) = [\tilde{E}_p(d+1) - \tilde{E}_p(d)]/T$ yields a reliable estimation of h_{KS} .

A final issue has to be solved: how can one calculate $\tilde{e}_p(d)$ when D is not known? D can be estimated through the Kaplan–Yorke formula⁶⁵, but this in turns requires knowing the Lyapunov exponents of the system. The solution entails substituting D with an unknown parameter δ , yielding $\tilde{e}_p(d, \delta)$ —note that the standard permutation entropy is recovered for $\delta = 0$. When $\delta < D$ ($\delta > D$), $\tilde{e}_p(d, \delta)$ will converge to the asymptotic value h_{KS} from above (respectively, from below). Therefore, D can be estimated as the value of δ such that $\tilde{e}_p(d, \delta)$ is independent of d .

This approach, although theoretically powerful, presents two important drawbacks. First of all, it is theoretically complex and requires a deep understanding of dynamical systems. Second, it requires long time series, as $\tilde{e}_p(d)$ is given by an asymptotic process for large values of d —which leads back to the condition $l \gg (d+1)$ ⁵¹. These are probably the reasons why, to the best of our knowledge, this approach has never been applied to the study of real-world time series.

Successions of permutation patterns. If all previous methodologies were based on the analysis of the appearance of permutation patterns taken in an isolated way, another possibility is available: consider how they follow one another. Specifically, let us consider a time series x_t , and the corresponding sequence of permutation patterns π_t . Transitions between patterns can be evaluated as the number of times (or the probability) that a given permutation pattern is followed by a second one. To illustrate, the time series $x = (1, 2, 3, 4)$ will have the pattern $\pi_{t=1} = (1, 2, 3)$ followed by $\pi_{t=2} = (1, 2, 3)$. This can then be mapped into a ordinal patterns transition graph G_m whose element $g_{i,j}$ is the probability that pattern j follows pattern i .

A few observations have to be made on this mathematical object. First of all, it is associated with an important increase in the dimensionality of the problem, i.e. one moves from having $d!$ patterns (where d is the embedding dimension) to $d!^2$ transitions.

This allows for a much richer description of the system's dynamics but also implies that longer time series are needed, in order to achieve reliable results. Second, elements of G may not be independent. To illustrate, let us consider the time series $x = (1, 2, 3, y)$, where y can be any value. Independently on the value of y , the second pattern will never be $\pi = (3, 2, 1)$, i.e. a monotonic decreasing pattern, as the last part of the previous pattern (i.e. (2, 3)) constrains the initial part of the second one. This can easily be solved through two different strategies. First, by considering non-overlapping patterns, such that, for an embedding dimension of d , only patterns $\pi_t, \pi_{t+d}, \pi_{t+2d}, \dots$ are analysed. Second, by using an embedding delay $\tau > 1$, to also ensure that consecutive patterns are calculated over different data. On the other hand, the calculation of this transition graph inherits the main advantages of the permutation pattern methodology: its conceptual simplicity, the reduced computational cost, especially when compared to other graph-based techniques^{13,66–68}, and its robustness against noisy data.

The concept of transitions has first been proposed by Small in 2013⁴⁴ and consisted in identifying those permutation patterns that followed each other. Note that the resulting structure (i.e. a network) was undirected and unweighted, that is, pattern transitions probabilities were disregarded. Different dynamical systems, including chaotic maps and stochastic systems, were then identified by calculating the ordinal pattern length that maximised the amount of information in the network.

Transitions were then exploited by Borges et al.⁴⁸, who specifically focusses on the probability of self-transitions—i.e. when a pattern is followed by the same one. Authors propose a metric assessing the probability of self-transitions, i.e.

$$p_{st} = p(\pi_i, \pi_i) = \sum_i g_{i,i}. \quad (3)$$

p_{st} is trivially equal to $1/d!$ for completely random time series (provided $\tau > 1$ and the time series is long enough), as a permutation pattern can be followed by any other one with the same probability. Nevertheless, p_{st} increases with the determinism of the time series, making it easy to detect different types of coloured noise and chaotic systems. This is used to construct a discrimination model, based on the application of support vector machines on the parameters of a fit of the evolution of p_{st} as a function of τ , giving excellent classification scores⁴⁸.

Leveraging on a similar idea, Olivares et al.⁶⁹ propose to look at the local and global dynamics of transition patterns. Specifically, they propose the use of two metrics. The first one is the minimum pattern entropy, where the entropy of each pattern is calculated through the distribution probability of the patterns following it. The second metric is the conditional permutation entropy of the whole transition matrix, calculated as the sum of each pattern entropy weighted by its stationary distribution. Note that the former metric described the local (i.e. pattern-centric) dynamics, while the latter the global one. Additionally, by leveraging on the similarity with the concept of networks, both metrics are also called node and network entropies. The final result is a pair of values for each time series, which can then be represented in a bi-dimensional plane—an approach that will largely be exploited in the next section.

In spite of the conceptual simplicity of this approach, few real-world applications have been proposed. Beside the examples included in the original papers^{44,48,69}, the interested reader can also refer to the use of permutation pattern transitions to characterise electrocardiogram data⁷⁰.

When permutation patterns meet other metrics

If the entropy and variability of the distribution associated with permutation patterns have proven to be useful, there is also a

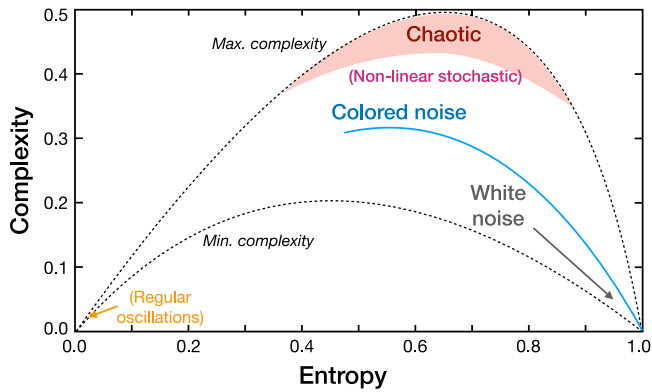


Fig. 2 Graphical representation of the complexity-entropy plane. Graphical representation of the plane as proposed by Rosso et al.⁷¹, and of the approximate position of chaotic systems, and coloured and white noises. Dynamics in parenthesis (i.e. non-linear stochastic and regular oscillations) were not included in the original work.

natural limit in the amount of information that can be conveyed by a single metric. A natural evolution is then to consider multiple (complementary) metrics at the same time and represent them as points in a plane (or a space). In this section, we review the planes that have been proposed in the literature, starting from the celebrated complexity-entropy plane.

The original complexity-entropy plane. The first example of a complexity-entropy plane was proposed by O. Rosso and co-authors⁷¹. Time series are characterised by two values, which are used to position them in a bi-dimensional plane. The first one is the classical permutation entropy, normalised in the interval [0, 1]: $E_S[P] = S[P]/S_{\max}$, where P is the distribution created by the permutation patterns, S the classical Shannon entropy, and $S_{\max} = \log_2 N$. (Note that the original work⁷¹ uses natural logarithms, as opposed to logarithms in base 2 common in information theory.) The second metric is the intensive statistical complexity measure $C_{JS}[P]$, defined as:

$$C_{JS}[P] = Q_J[P, P_e]E_S[P]. \tag{4}$$

Q_J is a measure of disequilibrium, i.e. of how far away is the distribution created by permutation patterns to an uniform distribution P_e , as is calculated through the well-known Jensen-Shannon (JS) divergence^{72,73}:

$$Q_J[P, P_e] = Q_0 \left\{ S\left[\frac{P + P_e}{2}\right] - \frac{S[P]}{2} - \frac{S[P_e]}{2} \right\}, \tag{5}$$

with Q_0 being a normalisation constant. Q_J is thus greater than zero if some permutation patterns are “privileged”, in the sense that they appear with a frequency higher than expected. It is important to note that this complexity measure goes beyond a simple entropy, as it assesses both the randomness and the correlation structures within the time series. Thanks to this, multiple values of C_{JS} can be obtained for each value of E_S , as was previously demonstrated⁷⁴.

When time series are located in the C_{JS} - E_S plane, several patterns are observed. First, chaotic systems have entropies between 0.45 and 0.7, and complexities close to maximum, owing to their internal correlation structures. Second, time series of white noise have maximum entropy and minimum complexity, as one may expect. Finally, coloured noises position themselves in the middle, with medium complexity and medium-high entropy values. A graphical representation of these regions is reported in Fig. 2, along with two additional dynamics not included in the original work⁷¹. It is worth noting that, besides these prototypical

examples, the position of a dynamical system in the plane will depend on the characteristics of the associated time series. To illustrate, let us consider the case of stochastic oscillations: the position will be dictated by the interaction between the sampling frequency and the multiple scales of the dynamics. At high sampling frequencies, what are observed are oscillations, which will be located in the bottom left corner of the plane; on the other hand, for samplings close to the main frequency of the system, the result will appear as noise, located in the bottom right corner. Varying the sampling frequency between these two extrema will give rise to complex movements in the plane⁴².

Besides being the foundation of the other methods described in this section, the complexity-entropy plane has buttressed a huge number of real-world analyses, owing to its theoretical and computational simplicity. These include applications in economy and finance, including stock^{22,75}, bond^{76,77}, cryptocurrencies^{78,79} and commodity market analyses⁸⁰; characterisation of lasers dynamics^{46,47,81}; of plasma and solar wind⁸²⁻⁸⁶; turbulence phenomena⁸⁷; stream flows⁸⁸⁻⁹⁰; the study of the dynamics of the brain⁹¹ and of its cells^{92,93}; of the dynamics of blood cells⁹⁴; the characterisation of ocean ambient noise⁹⁵; flame front dynamics⁵⁷ and of vehicle behaviour⁹⁶. It has even been applied to problems in image recognition^{97,98} and art⁹⁹.

The Fisher-entropy plane. Olivares et al.¹⁰⁰ proposed a modified version of the previously seen complexity-entropy plane by substituting the complexity by the discrete and normalised version of the Fisher’s Information Measure (FIM)¹⁰¹. This latter is defined as:

$$F[P] = F_0 \sum_{i=1}^{N-1} [(p_{i+1})^{1/2} - (p_i)^{1/2}]^2, \tag{6}$$

where F_0 is a suitable renormalisation coefficient. While related to the Shannon’s entropy, FIM presents an important difference: it is defined as a function of the difference in probability between consecutive elements of the distribution, as opposed to their raw value—or, in other words, as the distance between two contiguous probabilities. FIM is thus zero when all probabilities p are the same, and maximal when one single $p = 0$ —i.e. essentially the opposite of what would be expected in the case of the Shannon’s entropy. When compared to the original complexity-entropy plane, this new plane allows for a better characterisation of the dynamical changes induced by modifications in the system’s parameter, and it is able to distinguish between different types of chaotic dynamics¹⁰⁰.

The idea introduced by Olivares and co-workers¹⁰⁰ has seen real-world applications in several works, spanning from neural networks⁹² and electroencephalography (EEG) signal^{102,103} analysis, ecosystems’ dynamics¹⁰⁴, status of mechanical machines¹⁰⁵ and image recognition⁹⁸. It is also worth noting that the Fisher-entropy plane has inspired the so-called Fisher-DisEn plane¹⁰⁶, which uses the dispersion entropy¹⁰⁷ instead of the classical Shannon’s one.

Multi-scale planes. In all the previous methods, the embedding delay τ is considered as a fixed value, and in most applications it is assumed that $\tau = 1$. This assumption is valid provided that the system is temporally discrete (i.e. we observe the system at discrete time moments) and that the observation frequency is correctly tuned to the system dynamics. It is nevertheless difficult to fulfil these conditions for some real and numerical systems. One may consider, for instance, the case of the human brain: while EEG data are usually recorded at 250 or 500 Hz, they present multiple characteristic time scales that are condition

dependent^{108,109}. Analysing the raw data with a fixed τ may therefore lead to incomplete, or even misleading, results.

A solution to this problem was proposed through the definition of a multi-scale complexity–entropy plane⁴². Given a system, the two metrics of complexity C_{JS} and entropy E_S of the standard complexity–entropy plane are calculated as a function of τ , which is no longer fixed. The result is a parametric curve complexity–entropy plane, characterising the system through the two metrics with the embedding delay as parameter. In the case of most real-world applications, this implies calculating $C_{JS}(\tau)$ and $E_S(\tau)$ for $\tau = [1, 2, \dots]$; on the other hand, when the system under analysis is time continuous, τ can assume any fractional value greater than zero. A similar analysis was later performed⁴³, fixing τ but varying the sampling time in low-dimensional continuous chaotic systems.

As an example of an application, Zunino et al.⁴² resorted to the well-known Mackey–Glass equation, a paradigmatic time-delay system¹¹⁰; the embedding delay for which the complexity $C_{JS}(\tau)$ is maximal corresponds to the characteristic temporal scale of the equation, i.e. the minimally required sampling rate to capture all the information related to the non-linear correlations. Zunino et al.⁴² also applied this multi-scale plane to several real-world examples, including laser, river flow, geophysical, climate and financial data. Other examples include turbulence analysis^{87,111}, stream flows⁸⁹, flame front dynamics⁵⁷ and laser beam wandering¹¹². Still, one has to note that the line dividing this multi-scale approach from the standard complexity–entropy plane is fuzzy, as many works using the latter include some analysis on the sensitivity to the embedding delay τ .

Finally, it is worth noting that the work of Zunino and colleagues⁴² inspired a modification of the plane, called the *multi-scale weighted complexity entropy causality plane*^{17,113}, in which permutation patterns probabilities are weighted according to the amplitude of the signals generating them.

Additional mono-parametric complexity–entropy curves. What was introduced by Zunino et al.⁴² and previously discussed can be seen as a parametrisation of the complexity and entropy metrics, specifically as a function of the embedding delay τ . Yet, more parametrisations are possible¹¹⁴. Specifically, Ribeiro and co-workers propose to substitute the Shannon entropy with a monoparametric entropy, and specifically with the Tsallis q entropy¹¹⁵, defined as:

$$S_q(P) = \sum_{j=1}^d p_j \ln_q \frac{1}{p_j}. \tag{7}$$

In the previous equation, p_j is the appearance probability of pattern j , q is a real parameter and, finally, \ln_q is the q logarithm: $\ln_q x = \int_1^x t^{-q} dt$. In a similar way, the JS divergence of Rosso et al.⁷¹ is substituted by a generalisation of Kullback–Leibler divergence defined as: $K_q(P|R) = -\sum p_i \ln_q r_i/p_i$.

Instead of a single point, time series are now described by a curve, which displays an interesting feature: for stochastic time series it form loops, while this does not happen for chaotic time series in all embedding dimensions. The absence of a loop is a consequence of the absence of some patterns; therefore, this approach can be seen as a more complete variant of the missing pattern one⁵⁰. Beyond this, the characterisation of the curves in the plane can also be used to extract other properties of the time series, most notably the Hurst exponent¹¹⁴.

Ribeiro et al.¹¹⁴ applied this approach to several real-world time series, including laser dynamics, crude oil prices, sunspot index, heart dynamics and Earth’s magnetic activity. Other applications include the study of the dynamics of a real estate market¹¹⁶ and the analysis of EEG signals¹¹⁷.

Similarly to the Tsallis entropy case, another generalisation has been proposed¹¹⁸, based on substituting the Shannon’s entropy for the Rényi’s one. This is defined as:

$$S_r(P) = \frac{1}{1-r} \log \sum_{i=1}^n p_i^r, \tag{8}$$

where r is the so-called entropic index¹¹⁹. Due to the monotonic nature of S_r , curves in the Rényi complexity–entropy plane do not form loops. Still, their curvature is able to discriminate between stochastic, chaotic and period time series.

It is finally worth noting that both approaches have been merged under the form of three planes based on combining Tsallis and Rényi’s complexity and entropy metrics¹²⁰. Nevertheless, as the underlying distributions are obtained through the power spectrum of the signal and not through permutation patterns, this approach is not further described here.

The Tarnopolski plane. In 2016, M. Tarnopolski introduced a plane to characterise time series that, while having been developed independently, is still indirectly based on the concept of permutation patterns¹²¹. This plane is defined by two metrics:

1. The Abbe value \mathcal{A} , i.e. half of the ratio of the mean square successive difference to the variance^{122,123}:

$$\mathcal{A} = \frac{n}{2(n-1)} \frac{\sum_{i=1}^{n-1} (x_{i+1} - x_i)^2}{\sum_{i=1}^n (x_i - \bar{x})^2}, \tag{9}$$

with \bar{x} being the mean of $\{x_i\}$. \mathcal{A} quantifies the smoothness of the time series, spanning between zero (perfectly smooth) to one (white noise).

2. The probability \mathcal{T} of finding a turning point, i.e. when, in three consecutive observations, the middle value x_i is lower or higher than the two surrounding ones (x_{i-1} and x_{i+1}). Note that \mathcal{T} can easily be interpreted in the light of permutation patterns, as it is equivalent to the probability of four of the six possible patterns for $d = 3$.

While only the relation between the position in this $\mathcal{A} - \mathcal{T}$ plane and the Hurst exponent was originally studied¹²¹, Zunino et al.¹²⁴ builds on this to show that the plane is also capable of discriminating between different types of complex time series. Additionally, the authors of this last paper introduced a multi-scale version of the $\mathcal{A} - \mathcal{T}$ plane, based on downsampling the original time series using subwindows and on calculating the position on the plane as a function of the subwindow size. In spite of the simplicity of this approach, it has been applied to the study of few real-world time series, including the analysis of stock markets, electroencephalography and heart dynamics¹²⁴, and of stellar variability¹²⁵.

Building a full pipeline. All the previous discussed methodologies for detecting chaotic dynamics are based on the assumption that a researcher is controlling the process and thus that uncommon situations are manually discarded. To illustrate, a periodic dynamics will probably present missing (or less frequent) permutation patterns and may thus be classified as chaotic; yet, a simple graphical representation would discard this option. A final question may therefore be: can a fully automated pipeline be constructed, able to discriminate between stochastic, chaotic and periodic dynamics without external intervention?

Token et al.¹²⁶ proposed a solution to this question under the form of a decision tree³⁵. As a first step, they propose to exclude the possibility of stochasticity by comparing the permutation entropy of the original time series with that of two sets of surrogates: the Amplitude Adjusted Fourier Transform¹²⁷ and the Cyclic Phase Permutation¹²⁸. If the permutation entropy falls

within one of these two distributions, then the time series is classified as stochastic. If this is not the case, a few additional steps are executed. The signal is denoised, through the Schreiber's algorithm¹²⁹, and downsampled if an oversampling is detected. Finally, a modified version of the 0–1 test^{130,131} is applied, and the time series is classified as either chaotic or periodic. With the exception of a few free parameters, which are calibrated using a large collection of test time series, this pipeline allows to classify signals without any expert judgement.

Comparison of performance and cost

To compare the performance of all methodologies addressed in this review, we have considered three discrete chaotic dynamics and a linearly correlated stochastic process:

- *Chaotic logistic map.* Paradigmatic example usually employed as a testing ground to illustrate new concepts in the treatment of dynamical systems. It is a polynomial mapping of degree two¹³²: $x_{n+1} = r x_n(1 - x_n)$. We here consider its chaotic regime when $r = 4$.
- *Linear congruential generator.* 1D map, $x_{n+1} = A x_n + B \text{ mod}(C)$, normally used to produce pseudo-random integers in the range $0 < X_n < C$, which makes its classification a challenging task. Here we consider $A = 7141$, $B = 54773$ and $C = 259200$ ¹³³.
- *Sinai map.* Two-dimensional attractor, defined as $x_{n+1} = x_n + y_n + \delta \cos(2\pi y_n) \text{ mod}(1)$, $y_{n+1} = x_n + 2y_n \text{ mod}(1)$. Here we consider $\delta = 0.1$, for which a totally developed chaotic dynamics is obtained¹³³.
- *Noises with $1/f^k$ power spectrum.* Starting from a pseudo random variable with Gaussian distribution probability function, the desired power spectrum is obtained by the Fourier filtering method¹²⁷. Note that the degree of long-term correlations is directly proportional to k .

For the systems listed above, we have generated 10 independent realisations of 10^5 data samples, after discarding the first 10^5 iterations of the chaotic maps to avoid any transient behaviour. Each realisation started with different random initial conditions. The following analyses report the mean value over the realisations of the different metrics. Additionally, a noisy chaotic environment is generated by adding white Gaussian noise of zero mean to the original noise-free chaotic sequences. Different noise levels σ , defined by the ratio between the standard deviation of the noise and the original data, were considered. Ordinal patterns were evaluated with $D = 5$ and lag $\tau = 1$, except for estimating the probability of self-transitions for which $\tau > 1$ is required (as discussed in the section “Successions of permutation patterns”).

First, when seeking the presence of forbidden ordinal patterns we found that logistic chaotic dynamics and the x coordinate of the Sinai map are the only sequences that present forbidden patterns, on average 89 and 0.7, respectively. In fact, a minimum pattern length D is necessary to detect forbidden patterns in a noise-free deterministic dynamics¹³⁴. This drawback is the source of misclassifications of the underlying dynamical nature of the congruential map and the y coordinate of the Sinai map. Furthermore, a distinction between different correlation degrees for the k -noises cannot be achieved, since no forbidden patterns are observed for these stochastic processes. As previously seen, a more quantitative approach involves characterising the decay in the number of unobserved (forbidden or missing) ordinal patterns as a function of the sequence length. The corresponding results are depicted in Fig. 3a–e. As the weight of the noise component increases, all noisy chaotic maps locate in the same curve approximating to the bottom right corner, $B \sim 10^{-2}$ and

$\gamma \sim 1$ —parameters corresponding to an uncorrelated dynamics. Notably, decay rate allows identifying determinism even when the dynamics is noisy, with the noisy logistic map and the x -Sinai identified as chaotic up to noise levels 0.5 and 0.2, respectively—see Fig. 3b, d. On the other hand, the noisy congruential map and the y -Sinai share planar location with k -noises for all noise levels considered. However, for the y -Sinai sequence, temporal correlations are found for low noise contaminations—see Fig. 3e. Moreover, a quantification of the long-term correlations of k -noises are characterised by different planar locations.

Since a deterministic map may have no forbidden ordinal patterns for a given pattern length, another option is to focus on the shape of the distribution of visible ordinal patterns through χ^2 test with statistics given by Eq. 1. Figure 3f shows the distribution of χ^2 for 10^4 independent realisations. The rejection threshold of the null hypothesis H_0 (ordinal patterns are independent and identically distributed) at level $\alpha = 0.05$ is $\chi_{119,0.05}^2 = 145.46$. It is observed that, for the noisy logistic map and the Sinai map, χ^2 test rejects H_0 for all considered noise levels (except for the y -Sinai with $\sigma \sim 1$) with a high degree of confidence. On the other hand, for the congruential map, χ^2 test rejects H_0 only for the noise-free case. Lastly, for k -noises with $k < 0$, χ^2 test rejects H_0 , as can be seen in Fig. 3f. In synthesis, this approach is able to identify the determinism of all chaotic maps even in a noisy environment, except for the noisy congruential map. Yet, it lacks a distinction between chaos and stochastic dynamics.

Leaving the shape of the ordinal pattern distribution behind, it is now time to focus on its variability by applying the permutation spectrum test. The corresponding results are reported in Fig. 4. Free-noise chaotic maps exhibit substantial variability in the standard deviation of the spectrum. Particularly, the logistic map and the x -Sinai have ordinal patterns with zero deviation, due to the presence of forbidden/missing patterns—see Fig. 4a, c. On the contrary, the congruential map and the y -Sinai show some patterns with higher or lower standard deviation in comparison with the average, which demonstrate, at least, temporal correlation in the data—although a deterministic nature cannot be guaranteed, as can be seen in Fig. 4b, d. Linear correlated processes show a symmetric variability with no null values—see colour arrows in Fig. 4e–h. This symmetry reflects the reversibility of these linear processes. For $k = 0$, the standard deviation presents no variability, except for the first and last ordinal patterns. All ordinal patterns have the same probability of appearance, leading to a constant standard deviation. For studying a polluted chaotic dynamics, we have focussed on the noisy logistic map as it gives a more clear spectrum—see Fig. 4i–l. Noise contamination eliminates all forbidden patterns, but the “profile” of the standard deviation maintains robust. Even for high noise levels, some deviations are higher than the average—see black arrows in Fig. 4i–l. In synthesis, the permutation spectrum test, while quite sensitive, is rather qualitative in discriminating chaos from stochasticity, i.e. it requires a visual inspection of the results.

Following the structure of the previous part of the work, transitions between ordinal patterns are next, and specifically self-transitions p_{st} . The evolution of p_{st} has been analysed as a function of τ ($\tau \in [2, 50]$); after estimating the fitting parameters β_0 , β_1 and its error R^2 , as proposed by Borges et al.⁴⁸; the k -mean clustering algorithm of MATLAB© was used to classify the dynamical nature of the noisy chaotic maps and the k -noises. Figure 5a depicts the clustering obtained by the triplet $\{\beta_0, \beta_1, R^2\}$. Only two misclassifications, k -noises with $k = 0$ and 0.2, are observed, leading to an accuracy of 96.61%. The drawback of this (at first) excellent discrimination is that the Gaussian white noise is classified as chaotic. Note that the projection in the plane β_0 versus β_1 delivers a quantification of the degree of long-term linear correlations of the k -noises. The second option using transitions involves characterising

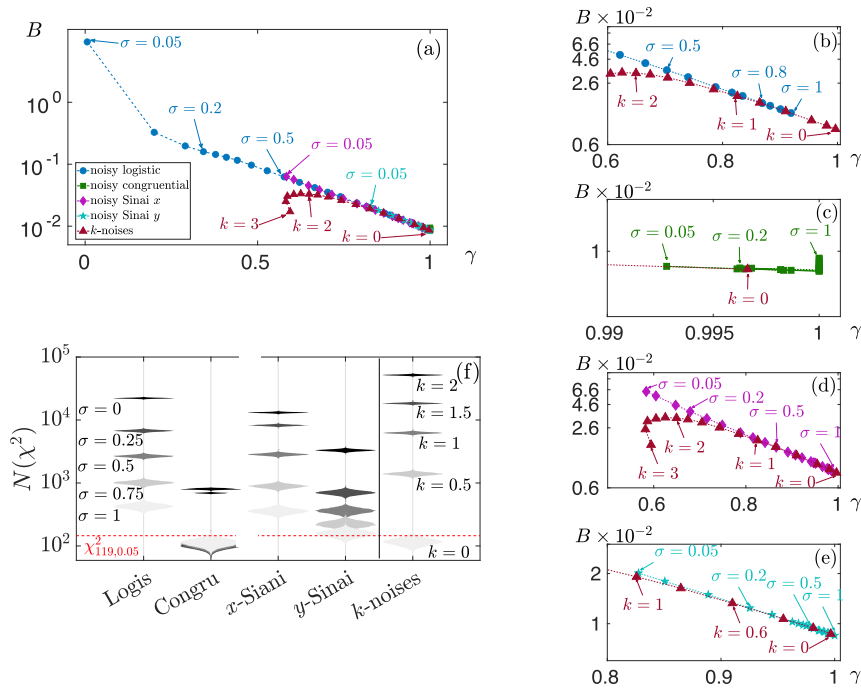


Fig. 3 Unobserved and distribution of visible ordinal patterns methodologies. **a** Characteristic decay rate B versus the stretched exponent γ for k -noises with $k \in [0, 3]$ with step 0.2 (solid brown triangles) and logistic map (solid blue circles), congruential map (solid green squares), x -Sinai (solid magenta diamonds) and y -Sinai (solid cyan stars) with additive noise with $\sigma \in [0, 1]$ with step 0.05. **b–e** Zoom of individual maps near the stochastic zone ($B \sim 10^{-2}$ and $\gamma \sim 1$). **f** Distribution $N(\chi^2)$ of χ^2 for 10^4 independent realisations of all the noisy chaotic maps with additive noise with $\sigma = 0.25, 0.5, 0.75$ and 1 , and k -noises with $k = 0, 0.5, 1, 1.5$ and 2 . Dashed red line indicates the threshold $\chi^2_{D-1, \alpha}$, for $D = 5$ and $\alpha = 0.05$. k : correlation degree and σ : intensity of the noise contamination.

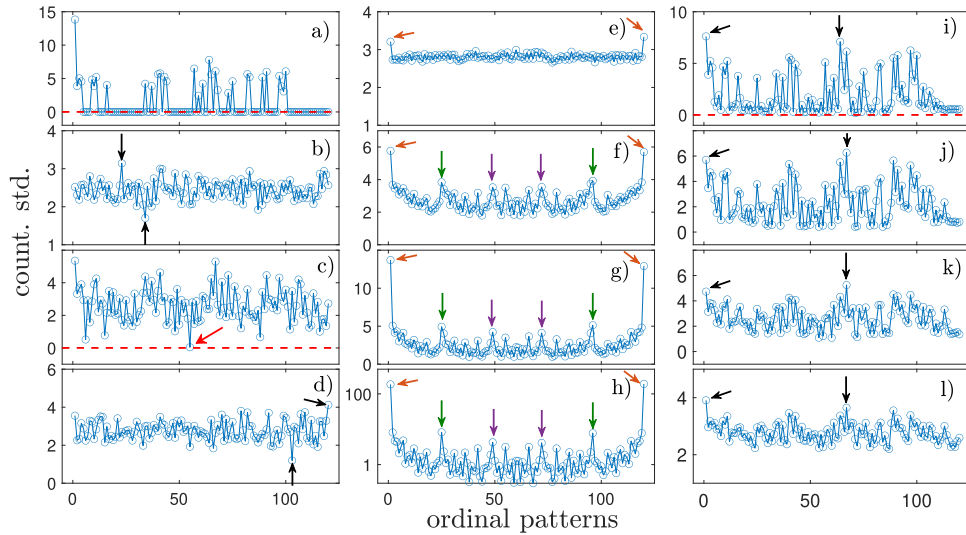


Fig. 4 Standard deviation permutation spectrum. Standard deviation of the permutation spectrum estimated from 200 windows of size $l = 10^3$ and for **a** the logistic map, **b** the linear congruential generator, **c** x and **d** y coordinate of the Sine map. k -noises for **e** $k = 0$, **f** $k = 1$, **g** $k = 2$ and **h** $k = 3$. **i–l** Noisy chaotic logistic map with additive noise with $\sigma = 0.25, 0.5, 0.75$ and 1 , respectively. Red dashed line indicates zero standard deviation and arrows point out characteristic ordinal patterns. k : correlation degree and σ : intensity of the noise contamination.

the local and global features of the transition matrix of all ordinal transitions, by plotting the minimum pattern entropy versus the conditional permutation entropy⁶⁹. This representation plane places all chaotic maps below the k -noises, the latter ones locating near the diagonal—see Fig. 5b. As noise level increases, the positions of chaotic systems get closer to the linear stochastic one. This characterisation identifies the presence of forbidden patterns with null value of the minimum pattern entropy, as the case of logistic map.

Note that the determinism of the congruential map is appropriately contrasted with linear stochastic dynamics by its location.

Global and local features of the stationary ordinal pattern distribution can be characterised by the complexity–entropy and Fisher–entropy planes, respectively—see Fig. 6. In the former plane, the noisy logistic dynamics is distinguished from k -noises up to approximately 0.4 of noise level, as evidenced in Fig. 6ai–ei. However, the rest of the chaotic maps overlap with the stochastic

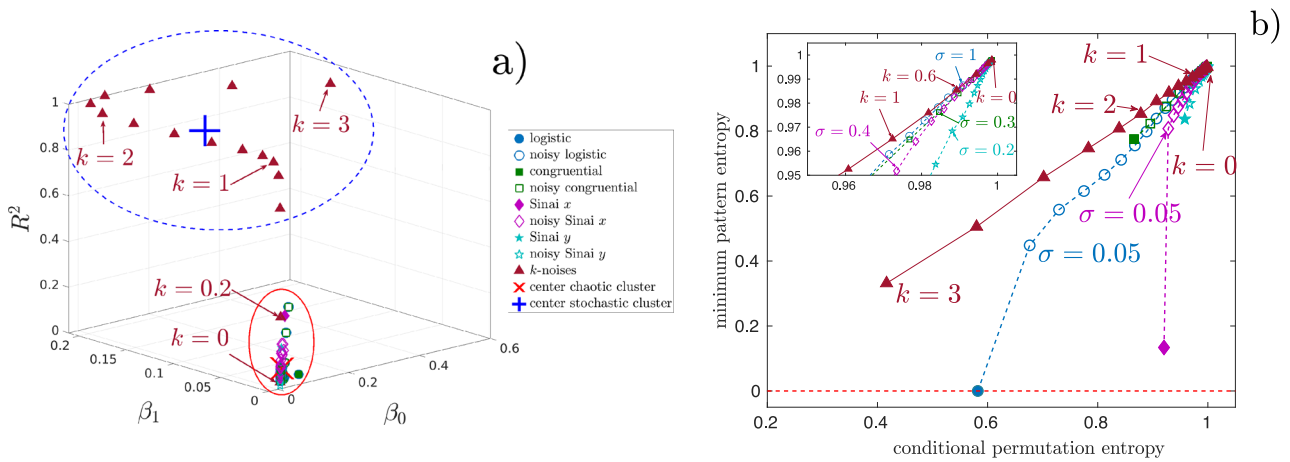


Fig. 5 Ordinal transition approaches. **a** Clustering representation of the triplet $\{\beta_0, \beta_1, R^2\}$ (β_0 and β_1 being parameters of the model applied to $p_{st}(\tau)$ defined in ref. 48 and R^2 stands for the error of the fitted model) and **b** minimum pattern entropy versus conditional permutation entropy for k -noises ($k \in [0, 3]$ with step 0.2) and chaotic maps with additive noise with $\sigma \in [0, 1]$ with step 0.05. Results in **b** were obtained by using 10^6 data points to have a reliable contrast. Noise-free sequences (solid symbols). Noisy sequences (open symbols). k : correlation degree and σ : intensity of the noise contamination.

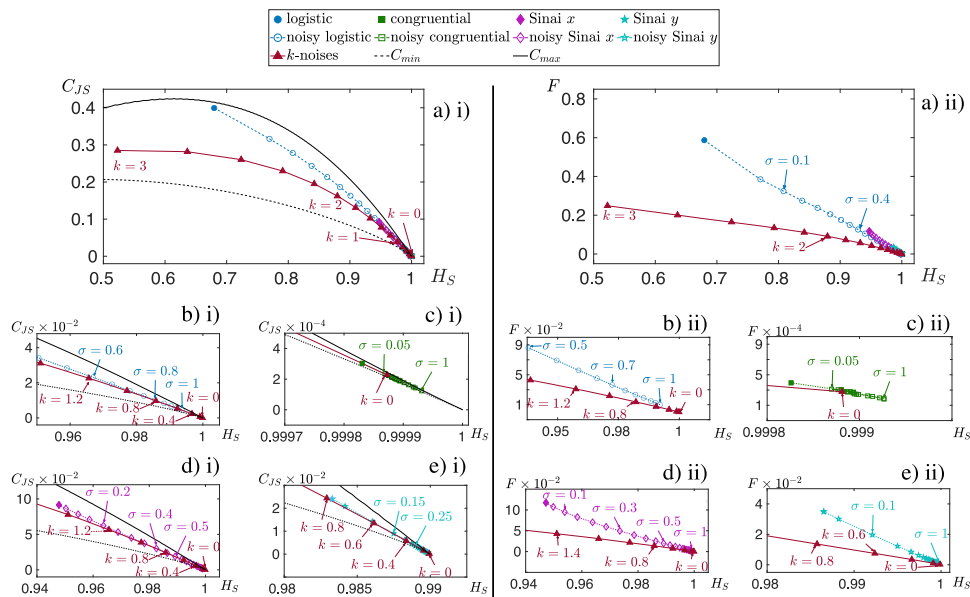


Fig. 6 Global versus local representation planes. Localisation of the k -noises ($k \in [0, 3]$ with step 0.2) and chaotic maps in the **ai** permutation complexity-entropy plane and **a ii** Fisher-entropy plane. Additive noise with $\sigma \in [0, 1]$ with step 0.05 is been depicted. Noise-free sequences (solid symbols). Noisy sequences (open symbols). Zoom of individual maps near the stochastic zone: **bi, bii** logistic map, **ci, -cii** congruential map, **di, dii** x-Sinai and **ei, eii** y-Sinai. k : correlation degree and σ : intensity of the noise contamination.

curve, even for noise-free sequences. When local aspects of the distribution are taken into account by the Fisher information, we found a clearer contrast between different dynamics, even for high observational noise pollution—see Fig. 6aii–eii. Both planes characterise the congruential map as slightly correlated dynamics. Another way of incorporating local features is through the q -parametric curves in the q -complexity-entropy plane. Figure 7a–d shows the loops formed by the k -noises, the hallmark of stochasticity. The absence of a loop is only found for the noise-free logistic map and the x -Sinai—see Fig. 7e, g. Since a closed q -curve is based on the existence of forbidden patterns, this methodology fails to detect determinism in the chaotic sequences that materialise all ordinal patterns for a given D , as is the case of the congruential map, the y -Sinai and the noisy logistic map, as observed in Fig. 7f, h. Lastly, we found that the Tarnopolski plane delivers a quite good quantification of the long-term correlations

of k -noises, especially for small values of k , as can be seen in Fig. 7i. Nevertheless, the contrast between an uncorrelated dynamics and a noisy chaotic dynamical is rather confused. This lies in the fact that a pattern length of $D = 3$ is not long enough to unveil determinism in a sequence.

As a last point, and with the aim of comparing the computational cost of all methodologies, we have calculated their running times when a totally uncorrelated Gaussian sequence of 10^6 data points is analysed using $D = 3, 4$ and 5 , and $\tau = 1$ in a MATLAB® implementation. Figure 8 shows the comparison between the running time averaged over 10 independent runs. The evaluation of the q -parametric curve in the entropy-complexity plane corresponds to the highest computational cost, since a large range of q values is needed to obtain the curves—see Fig. 7. The fitting procedure to estimate certain parameters of the corresponding model together with multi-scale analysis place the decay of the number of

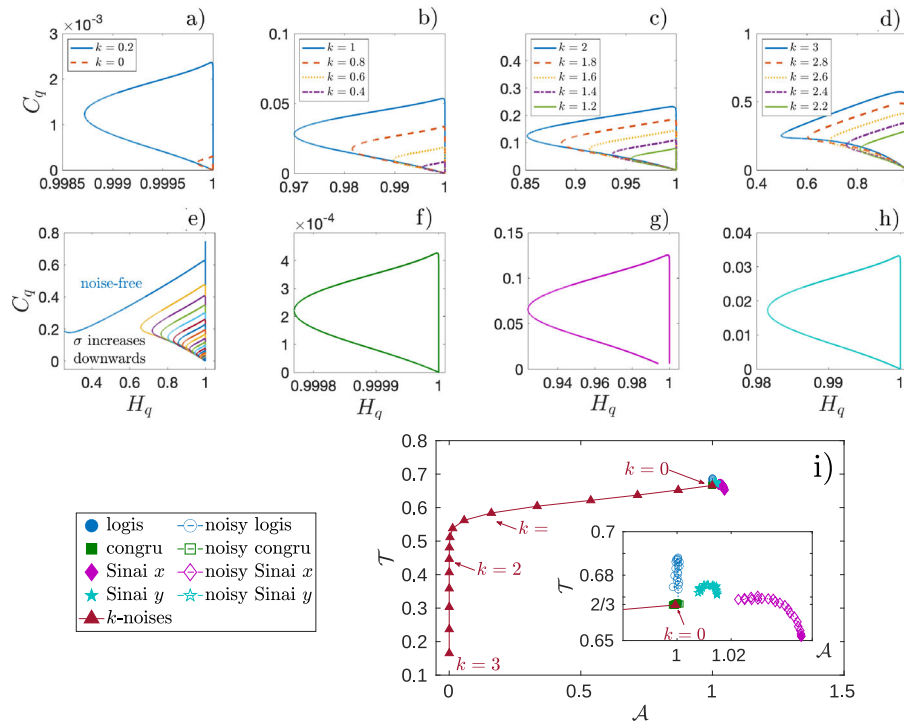


Fig. 7 q-parametrisation of the complexity-entropy plane and Tarnopolski plane. Entropy-complexity plane with $q \in [10^{-4}, 1] \cup [1, 10^3]$ with steps 10^{-3} and 10^{-2} , respectively, for k -noises with **a** $k = 0$ and 0.2 , **b** $k = 0.4, 0.6, 0.8$ and 1 , **c** $k = 1.2, 1.4, 1.6, 1.8$ and 2 , **d** $k = 2.2, 2.4, 2.6, 2.8$ and 3 , **e** logistic map with additive noise with $\sigma \in [0, 1]$ with step 0.05 , **f** linear congruential map, **g** x and **h** y coordinate of the Sinai map. **i** Turning point probability \mathcal{T} versus the Abbe number \mathcal{A} for k -noises ($k \in [0, 3]$ with step 0.2) and chaotic maps with additive noise with $\sigma \in [0, 1]$ with step 0.05 . Inset plot shows zoom near the stochastic zone ($\mathcal{T} = 2/3$ end $\mathcal{A} = 1$). Noise-free sequences (solid symbols). Noisy sequences (open symbols). k : correlation degree and σ : intensity of the noise contamination.

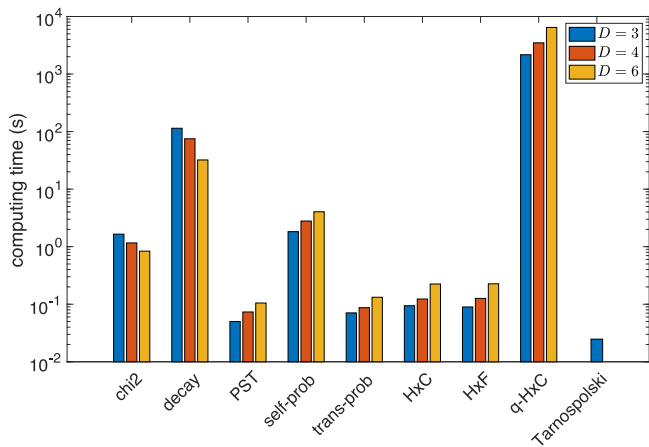


Fig. 8 Computational cost. Comparison between the computational cost of each methodology when analysing an uncorrelated Gaussian sequence of 10^6 data points using $D = 3, 4$ and 5 , and $\tau = 1$ (except for p_{st} , for which $\tau \in [1, 50]$). The averages over ten independent realisations are reported.

unobserved ordinal patterns and the self-probability approach as the second and third most costly algorithms, respectively. This is due to the fact that the former considers several sequence sizes, while the latter covers a wide range of values of τ ($\tau \in [2, 50]$). The rest of the algorithms have similar running times.

The limits of permutation patterns

Throughout this review, we have seen that permutation patterns and metrics from them derived can help distinguishing chaos from stochasticity in a wide array of conditions. Does this mean

that permutation patterns can be the universal panacea? Unfortunately, this is not the case, and the researcher should always be cautious about discarding a chaotic behaviour just on the basis of a single test. To illustrate this point, we here show how a simple map can ad hoc be built that is deterministic and sensitive to initial condition but still have permutation patterns compatible with a stochastic dynamics.

The main idea is to disentangle the sequence of permutation patterns from the values creating them, for thus generating a time series with a custom distribution of patterns. To illustrate, let us consider the permutation patterns for $d = 3$, as shown in Fig. 9a. Any sequence of three values $[x(t), x(t + 1), x(t + 2)]$ will be associated with a permutation pattern, which in turn constrains the next possible pattern. For instance, if the pattern is $(1, 2, 3)$ (i.e. $x(t) < x(t + 1) < x(t + 2)$), the following one can only be $(1, 2, 3), (1, 3, 2)$ or $(3, 1, 2)$. It is then possible to create a matrix with all the possible transitions between permutation patterns and a periodic sequence visiting all patterns with equal frequency —see Fig. 9b. Starting from one pattern, values have to be added to the time series according to the limits imposed by the next pattern. Therefore, if $x(t) < x(t + 1)$ and the pattern to be fulfilled is $(1, 2, 3)$, the following value has to be in the range $(x(t + 1), l_{sup}]$, where l_{sup} is the maximum value of the map. As an example, we are here using a logistic map $y(t + 1) = 4y(t)[1 - y(t)]$, with $y(0) = x(0)$ the initial condition of the map. Going back to the previous example, the third value used to fulfil the pattern $(1, 2, 3)$ will be $x(t + 2) = x(t + 1) + [1 - x(t + 1)]y(t + 1)$.

The resulting time series x has some interesting properties. First of all, it is a completely deterministic map, as $x(t + 1)$ is fully defined by $x(t)$ and $y(t)$, which are in turn fully defined by $x(0)$, i.e. by the initial condition. Second, the map inherits the strong sensitivity to initial conditions of the logistic map. Finally, and

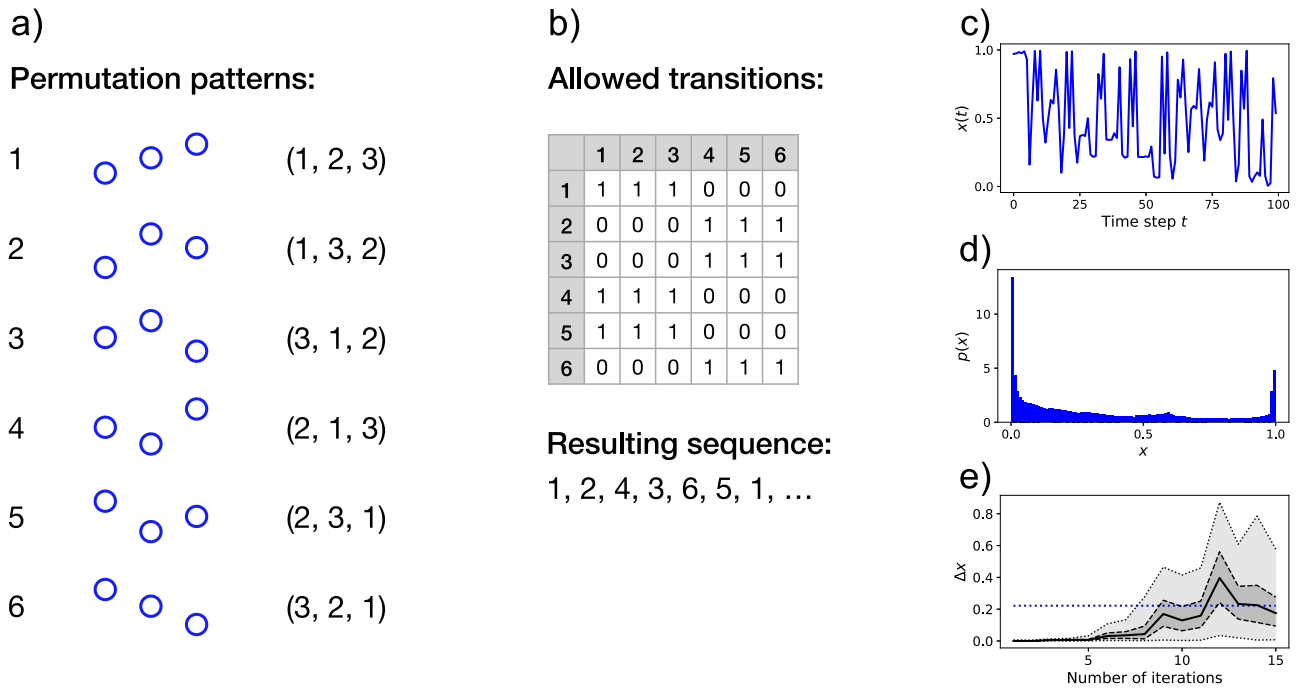


Fig. 9 Synthetic map. Constructing a synthetic chaotic map with a perfect distribution of permutation patterns. **a** Labelling of the six permutation patterns for $d = 3$. **b** Matrix representing the allowed transitions between permutation patterns and example of a possible periodic sequence of patterns. **c** Example of the time series that can be obtained from the previous sequence of permutation patterns. **d** Probability distribution of values for the resulting time series. **e** Sensitivity to initial conditions, calculated as the difference between two values of the resulting time series as a function of the number of iterations separating them. The solid black line indicates the median value, and dark and light grey bands, respectively, one and two standard deviations. The horizontal blue dotted line represents the expected value of the difference in a random time series with the same probability distribution.

most importantly here, it has a perfectly balanced distribution of permutation patterns, as by construction all of them are visited with equal frequency. This implies that any method based on single permutation patterns (i.e. not on transitions), e.g. on counting missing patterns, will wrongly classify this time series as stochastic. Similarly, any other measure based on patterns, as, for instance, irreversibility ones^{18,19}, will be misled. Note that this reconstruction method can easily be extended, for instance, to ensure that pattern transitions have equal probabilities.

Figure 9c reports an example of the resulting time series; Fig. 9d, an histogram of the value appearance probability, calculated over a time series with 10^6 points; and Fig. 9e, the distribution of the difference between the values of two time series, as a function of the number of iterations, when the initial values differ by 10^{-3} .

In synthesis, any method designed to discriminate between stochastic and chaotic time series is based on one or more hypotheses; in the case here considered, all methods assume that the chaotic nature of the underlying system manifests as an imbalance in the permutation patterns. While this is a reasonable assumption in most real-world systems, one must be cautious, as the presence of such imbalance is a sufficient but not necessary condition for a chaotic dynamics.

Conclusions and outlook

As shown in this review, many tests based on permutation patterns have been proposed to assess the chaotic versus stochastic nature of time series; whether one of them is clearly better than the other ones is nevertheless a complex question, with several aspects influencing the answer. Generally speaking, almost all methods are misled by the presence of observational noise, and this is especially relevant in the case of methods relying on the existence of forbidden ordinal patterns. These latter techniques,

including the classical entropy–complexity plane and its q -parameterised version, misclassify noise-free chaotic dynamics that materialise all ordinal patterns for a given value of D . Similarly, the permutation spectrum test yields a debatable characterisation for such kind of sequences. On the contrary, the decay of unobserved—forbidden or missing—ordinal patterns as a function of the sequence length gives a better characterisation, in the sense that allows quantifying the degree of linear correlations of stochastic processes and distinguishing them from noisy chaotic sequences. On the other hand, transitions between ordinal patterns unveil a sort of dynamical permutation hallmarks that differentiate, up to medium noise levels, linear stochastic processes from chaotic sequences, even for those having no forbidden patterns. This is the case of the representation plane defined by the minimum pattern entropy versus the conditional permutation entropy; still, this method also presents the drawback of requiring longer time series to obtain reliable results, which could be a major limitation in real-world applications. Ordinal pattern distribution-based methodologies, such as χ^2 test introduced by Amigó and co-workers, are extremely robust against noise contamination, yet are only able to reject or accept the null hypothesis that the sequence is independent and identically distributed. Lastly, when considering highly polluted chaotic sequences, the Fisher-entropy plane stands out as the best option to contrast them from linearly correlated stochastic systems.

In spite of generally remarkable results, we believe that two barriers are preventing permutation patterns to be regarded as the gold standard in the detection of chaos. First of all, all methods here presented are implicitly based on the hypothesis that chaos reflects in an imbalance of permutation patterns, which in turn indicates the presence of a non-linearity¹³⁵. This can nevertheless not be the case, as shown in the section “The limits of permutation patterns”. Most of our knowledge about permutation patterns and derived metrics comes from numerical experiments.

Yet, from a stricter theoretical perspective, permutation entropy is not directly measuring chaos, nor permutation patterns represent temporal causal structures; even the relationship between this and the KS entropy is known only for a limited number of dynamical systems^{16,62}. A more complete theoretical foundation is clearly needed.

Second, the success hitherto achieved by permutation patterns will be the drive behind the development of even more sensitive tests. We speculate that this will be attained through two complementary paths. On one hand, novel tests will shift towards micro-scale analyses, e.g. towards the study of the dynamics of individual patterns and sequences thereof. This will only be a prolongation of the historical trend, which has already moved from initial macro-scale approaches (including entropies and missing patterns) to more localised ones (like transition probabilities). Focussing the attention to one or few permutation patterns will bring several benefits, including the reduction of the computational cost, hence the possibility of analysing structures at longer temporal scales; and eventually the creation of a catalogue of “chaotic fingerprints”. On the other hand, a second path may entail the combination of multiple and heterogeneous approaches into single tests, an option that only recently started to appear in the literature^{126,136}.

Data availability

No data sets were generated or analysed during the current study.

Received: 28 July 2020; Accepted: 5 August 2021;

Published online: 20 August 2021

References

- Nicolis, C. & Nicolis, G. Is there a climatic attractor? *Nature* **311**, 529–532 (1984).
- Grassberger, P. Do climatic attractors exist? *Nature* **323**, 609–612 (1986).
- Nicolis, C. & Nicolis, G. Evidence for climatic attractors. *Nature* **326**, 523–523 (1987).
- Hasselblatt, B. & Katok, A. *A First Course in Dynamics: With a Panorama of Recent Developments* (Cambridge University Press, 2003).
- Crutchfield, J. & Huberman, B. Fluctuations and the onset of chaos. *Phys. Lett.* **77A**, 407–410 (1980).
- Aurell, E., Boffetta, G., Crisanti, A., Paladin, G. & Vulpiani, A. Predictability in the large: an extension of the concept of lyapunov exponent. *J. Phys. A Math. Gen.* **30**, 1 (1997).
- Sigeti, D. E. Exponential decay of power spectra at high frequency and positive lyapunov exponents. *Phys. D* **82**, 136–153 (1995).
- Sugihara, G. & May, R. M. Nonlinear forecasting as a way of distinguishing chaos from measurement error in time series. *Nature* **344**, 734–741 (1990).
- Tsonis, A. & Elsner, J. Nonlinear prediction as a way of distinguishing chaos from random fractal sequences. *Nature* **358**, 217–220 (1992).
- Gautama, T., Mandic, D. P. & Van Hulle, M. M. The delay vector variance method for detecting determinism and nonlinearity in time series. *Phys. D* **190**, 167–176 (2004).
- Donner, R. V., Zou, Y., Donges, J. F., Marwan, N. & Kurths, J. Recurrence networks - a novel paradigm for nonlinear time series analysis. *N. J. Phys.* **12**, 033025 (2010).
- Donner, R. V. et al. Recurrence-based time series analysis by means of complex network methods. *Int. J. Bifurcation Chaos* **21**, 1019–1046 (2011).
- Lacasa, L., Luque, B., Ballesteros, F., Luque, J. & Nuno, J. C. From time series to complex networks: the visibility graph. *Proc. Natl Acad. Sci. USA* **105**, 4972–4975 (2008).
- Lacasa, L. & Toral, R. Description of stochastic and chaotic series using visibility graphs. *Phys. Rev. E* **82**, 036120 (2010).
- Bandt, C. & Pompe, B. Permutation entropy: a natural complexity measure for time series. *Phys. Rev. Lett.* **88**, 174102 (2002). **First work introducing the idea of permutation patterns.**
- Keller, K., Unakafov, A. M. & Unakafova, V. A. On the relation of ks entropy and permutation entropy. *Phys. D* **241**, 1477–1481 (2012). **Demonstration of the equivalence of the permutation and the Kolmogorov-Sinai entropies for some dynamical systems.**
- Fadlallah, B., Chen, B., Keil, A. & Principe, J. Weighted-permutation entropy: a complexity measure for time series incorporating amplitude information. *Phys. Rev. E* **87**, 022911 (2013).
- Zanin, M., Rodríguez-González, A., Menasalvas Ruiz, E. & Papo, D. Assessing time series reversibility through permutation patterns. *Entropy* **20**, 665 (2018).
- Martínez, J. H., Herrera-Diestra, J. L. & Chavez, M. Detection of time reversibility in time series by ordinal patterns analysis. *Chaos* **28**, 123111 (2018).
- Yao, W., Yao, W., Wang, J. & Dai, J. Quantifying time irreversibility using probabilistic differences between symmetric permutations. *Phys. Lett. A* **383**, 738–743 (2019).
- Zanin, M. Forbidden patterns in financial time series. *Chaos* **18**, 013119 (2008).
- Zunino, L., Zanin, M., Tabak, B. M., Pérez, D. G. & Rosso, O. A. Forbidden patterns, permutation entropy and stock market inefficiency. *Phys. A* **388**, 2854–2864 (2009).
- Nicolaou, N. & Georgiou, J. Detection of epileptic electroencephalogram based on permutation entropy and support vector machines. *Expert Syst. Appl.* **39**, 202–209 (2012).
- Zhang, X., Liang, Y. & Zhou, J. et al. A novel bearing fault diagnosis model integrated permutation entropy, ensemble empirical mode decomposition and optimized SVM. *Measurement* **69**, 164–179 (2015).
- Martin-Gonzalo, J.-A. et al. Permutation entropy and irreversibility in gait kinematic time series from patients with mild cognitive decline and early Alzheimer’s dementia. *Entropy* **21**, 868 (2019).
- Amigó, J. *Permutation Complexity in Dynamical Systems: Ordinal Patterns, Permutation Entropy and All That* (Springer Science & Business Media, 2010).
- Zanin, M., Zunino, L., Rosso, O. A. & Papo, D. Permutation entropy and its main biomedical and econophysics applications: a review. *Entropy* **14**, 1553–1577 (2012).
- Keller, K., Unakafov, A. M. & Unakafova, V. A. Ordinal patterns, entropy, and EEG. *Entropy* **16**, 6212–6239 (2014).
- Staniek, M. & Lehnertz, K. Parameter selection for permutation entropy measurements. *Int. J. Bifurcation Chaos* **17**, 3729–3733 (2007).
- Riedl, M., Müller, A. & Wessel, N. Practical considerations of permutation entropy. *Eur. Phys. J. Spec. Top.* **222**, 249–262 (2013).
- Zunino, L., Olivares, F., Scholkmann, F. & Rosso, O. A. Permutation entropy based time series analysis: equalities in the input signal can lead to false conclusions. *Phys. Lett. A* **381**, 1883–1892 (2017).
- Keller, K., Mangold, T., Stolz, I. & Werner, J. Permutation entropy: new ideas and challenges. *Entropy* **19**, 134 (2017).
- Berger, S., Schneider, G., Kochs, E. F. & Jordan, D. Permutation entropy: too complex a measure for EEG time series? *Entropy* **19**, 692 (2017).
- Cuesta-Frau, D., Varela-Entrecanales, M., Molina-Picó, A. & Vargas, B. Patterns with equal values in permutation entropy: do they really matter for biosignal classification? *Complexity* **2018**, 1324696 (2018).
- Moret, B. M. Decision trees and diagrams. *ACM Comput. Surv.* **14**, 593–623 (1982).
- Frank, B., Pompe, B., Schneider, U. & Hoyer, D. Permutation entropy improves fetal behavioural state classification based on heart rate analysis from biomagnetic recordings in near term fetuses. *Med. Biol. Eng. Comput.* **44**, 179 (2006).
- Watt, S. J. & Politi, A. Permutation entropy revisited. *Chaos Solitons Fractals* **120**, 95–99 (2019).
- Bian, C., Qin, C., Ma, Q. D. & Shen, Q. Modified permutation-entropy analysis of heartbeat dynamics. *Phys. Rev. E* **85**, 021906 (2012).
- Kulp, C., Chobot, J., Niskala, B. & Needhammer, C. Using forbidden ordinal patterns to detect determinism in irregularly sampled time series. *Chaos* **26**, 023107 (2016).
- McCullough, M., Sakellariou, K., Stemler, T. & Small, M. Counting forbidden patterns in irregularly sampled time series. I. The effects of under-sampling, random depletion, and timing jitter. *Chaos* **26**, 123103 (2016).
- Sakellariou, K., McCullough, M., Stemler, T. & Small, M. Counting forbidden patterns in irregularly sampled time series. II. Reliability in the presence of highly irregular sampling. *Chaos* **26**, 123104 (2016).
- Zunino, L., Soriano, M. C. & Rosso, O. A. Distinguishing chaotic and stochastic dynamics from time series by using a multiscale symbolic approach. *Phys. Rev. E* **86**, 046210 (2012).
- De Micco, L., Fernández, J. G., Larrondo, H. A., Plastino, A. & Rosso, O. A. Sampling period, statistical complexity, and chaotic attractors. *Phys. A* **391**, 2564–2575 (2012).
- Small, M. Complex networks from time series: capturing dynamics. In *2013 IEEE International Symposium on Circuits and Systems (ISCAS2013)* 2509–2512 (IEEE, 2013). **First work proposing the concept of analysing successions of permutation patterns.**
- Olivares, F., Zunino, L., Soriano, M. C. & Pérez, D. G. Unraveling the decay of the number of unobserved ordinal patterns in noisy chaotic dynamics. *Phys. Rev. E* **100**, 042215 (2019).

46. Soriano, M. C., Zunino, L., Rosso, O. A., Fischer, I. & Mirasso, C. R. Time scales of a chaotic semiconductor laser with optical feedback under the lens of a permutation information analysis. *IEEE J. Quant. Electron.* **47**, 252–261 (2011).
47. Soriano, M. C., Zunino, L., Larger, L., Fischer, I. & Mirasso, C. R. Distinguishing fingerprints of hyperchaotic and stochastic dynamics in optical chaos from a delayed opto-electronic oscillator. *Opt. Lett.* **36**, 2212–2214 (2011).
48. Borges, J. B. et al. Learning and distinguishing time series dynamics via ordinal patterns transition graphs. *Appl. Math. Comput.* **362**, 124554 (2019).
49. Olivares, F. & Zunino, L. Multiscale dynamics under the lens of permutation entropy. *Phys. A* **559**, 125081 (2020).
50. Amigó, J. M., Kocarev, L. & Szczepanski, J. Order patterns and chaos. *Phys. Lett. A* **355**, 27–31 (2006). **First example of the use of permutation patterns to discriminate between chaotic and stochastic time series.**
51. Amigó, J. M., Zambrano, S. & Sanjuán, M. A. True and false forbidden patterns in deterministic and random dynamics. *EPL (Europhys. Lett.)* **79**, 50001 (2007).
52. Amigó, J. M., Zambrano, S. & Sanjuán, M. A. F. Combinatorial detection of determinism in noisy time series. *EPL (Europhys. Lett.)* **83**, 60005 (2008).
53. Pukénas, K., Poderys, J. & Gulbinas, R. Measuring the complexity of a physiological time series: a review. *Baltic J. Sport Health Sci.* **1**, 48–54 (2012).
54. Humeau-Heurtier, A. The multiscale entropy algorithm and its variants: a review. *Entropy* **17**, 3110–3123 (2015).
55. Kulp, C. & Zunino, L. Discriminating chaotic and stochastic dynamics through the permutation spectrum test. *Chaos* **24**, 033116 (2014).
56. Tony, J., Gopalakrishnan, E., Sreelekha, E. & Sujith, R. Detecting deterministic nature of pressure measurements from a turbulent combustor. *Phys. Rev. E* **92**, 062902 (2015).
57. Gotoda, H., Kobayashi, H. & Hayashi, K. Chaotic dynamics of a swirling flame front instability generated by a change in gravitational orientation. *Phys. Rev. E* **95**, 022201 (2017).
58. Siddagangaiah, S., Li, Y., Guo, X. & Yang, K. On the dynamics of ocean ambient noise: two decades later. *Chaos* **25**, 103117 (2015).
59. Kolmogorov, A. N. Entropy per unit time as a metric invariant of automorphisms. *Dokl. Akad. Nauk SSSR* **124**, 754–755 (1959).
60. Ruelle, D. An inequality for the entropy of differentiable maps. *Boletim Soc. Bras. Mate. Bull.* **9**, 83–87 (1978).
61. Kamizawa, T., Hara, T. & Ohya, M. On relations among the entropic chaos degree, the Kolmogorov-Sinai entropy and the Lyapunov exponent. *J. Math. Phys.* **55**, 032702 (2014).
62. Bandt, C., Keller, G. & Pompe, B. Entropy of interval maps via permutations. *Nonlinearity* **15**, 1595 (2002).
63. Amigó, J. M., Kennel, M. B. & Kocarev, L. The permutation entropy rate equals the metric entropy rate for ergodic information sources and ergodic dynamical systems. *Phys. D* **210**, 77–95 (2005).
64. Politi, A. Quantifying the dynamical complexity of chaotic time series. *Phys. Rev. Lett.* **118**, 144101 (2017).
65. Kaplan, J. L. & Yorke, J. A. In *Functional Differential Equations and Approximation of Fixed Points* 204–227 (Springer, 1979).
66. Jin, R., McCallen, S. & Almaas, E. Trend motif: a graph mining approach for analysis of dynamic complex networks. In *Seventh IEEE International Conference on Data Mining (ICDM 2007)* 541–546 (IEEE, 2007).
67. Bezudnov, I. & Snarskii, A. From the time series to the complex networks: the parametric natural visibility graph. *Phys. A* **414**, 53–60 (2014).
68. Stephen, M., Gu, C. & Yang, H. Visibility graph based time series analysis. *PLoS ONE* **10**, e0143015 (2015).
69. Olivares, F., Zanin, M., Zunino, L. & Pérez, D. Contrasting chaotic with stochastic dynamics via ordinal transition networks. *Chaos* **30**, 063101 (2020).
70. Kulp, C. W., Chobot, J. M., Freitas, H. R. & Sprechini, G. D. Using ordinal partition transition networks to analyze ECG data. *Chaos* **26**, 073114 (2016).
71. Rosso, O., Larrondo, H., Martin, M., Plastino, A. & Fuentes, M. Distinguishing noise from chaos. *Phys. Rev. Lett.* **99**, 154102 (2007). **Seminal work introducing the concept of complexity-entropy plane.**
72. Grosse, I. et al. Analysis of symbolic sequences using the Jensen-Shannon divergence. *Phys. Rev. E* **65**, 041905 (2002).
73. Briët, J. & Harremoës, P. Properties of classical and quantum Jensen-Shannon divergence. *Phys. Rev. A* **79**, 052311 (2009).
74. López-Ruiz, R., Mancini, H. & Calbet, X. A statistical measure of complexity. *Phys. Lett. A* **209**, 321–326 (1995).
75. Zunino, L., Zanin, M., Tabak, B. M., Pérez, D. G. & Rosso, O. A. Complexity-entropy causality plane: a useful approach to quantify the stock market inefficiency. *Phys. A* **389**, 1891–1901 (2010).
76. Zunino, L., Bariviera, A. F., Guercio, M. B., Martínez, L. B. & Rosso, O. A. On the efficiency of sovereign bond markets. *Phys. A* **391**, 4342–4349 (2012).
77. Bariviera, A. F., Zunino, L., Guercio, M. B., Martínez, L. B. & Rosso, O. A. Efficiency and credit ratings: a permutation-information-theory analysis. *J. Stat. Mech. Theory Exp.* **2013**, P08007 (2013).
78. Bariviera, A. F., Zunino, L. & Rosso, O. A. An analysis of high-frequency cryptocurrencies prices dynamics using permutation-information-theory quantifiers. *Chaos* **28**, 075511 (2018).
79. Sigaki, H. Y., Perc, M. & Ribeiro, H. V. Clustering patterns in efficiency and the coming-of-age of the cryptocurrency market. *Sci. Rep.* **9**, 1–9 (2019).
80. Zunino, L. et al. Commodity predictability analysis with a permutation information theory approach. *Phys. A* **390**, 876–890 (2011).
81. Tiana-Alsina, J., Torrent, M., Rosso, O., Masoller, C. & Garcia-Ojalvo, J. Quantifying the statistical complexity of low-frequency fluctuations in semiconductor lasers with optical feedback. *Phys. Rev. A* **82**, 013819 (2010).
82. Maggs, J. & Morales, G. Permutation entropy analysis of temperature fluctuations from a basic electron heat transport experiment. *Plasma Phys. Controlled Fusion* **55**, 085015 (2013).
83. Gekelman, W., Van Compernelle, B., DeHaas, T. & Vincena, S. Chaos in magnetic flux ropes. *Plasma Phys. Controlled Fusion* **56**, 064002 (2014).
84. Weck, P. J., Schaffner, D. A., Brown, M. R. & Wicks, R. T. Permutation entropy and statistical complexity analysis of turbulence in laboratory plasmas and the solar wind. *Phys. Rev. E* **91**, 023101 (2015).
85. Maggs, J., Rhodes, T. L. & Morales, G. Chaotic density fluctuations in I-mode plasmas of the diii-d Tokamak. *Plasma Phys. Controlled Fusion* **57**, 045004 (2015).
86. Zhu, Z., White, A., Carter, T., Baek, S. G. & Terry, J. Chaotic edge density fluctuations in the alcator c-mod tokamak. *Phys. Plasmas* **24**, 042301 (2017).
87. Li, Q. & Zuntao, F. Permutation entropy and statistical complexity quantifier of nonstationarity effect in the vertical velocity records. *Phys. Rev. E* **89**, 012905 (2014).
88. Lange, H., Rosso, O. A. & Hauhs, M. Ordinal pattern and statistical complexity analysis of daily stream flow time series. *Eur. Phys. J. Spec. Top.* **222**, 535–552 (2013).
89. Serinaldi, F., Zunino, L. & Rosso, O. A. Complexity-entropy analysis of daily stream flow time series in the continental United States. *Stoch. Environ. Res. Risk Assess.* **28**, 1685–1708 (2014).
90. Stosic, T., Telesca, L., de Souza Ferreira, D. V. & Stosic, B. Investigating anthropically induced effects in streamflow dynamics by using permutation entropy and statistical complexity analysis: a case study. *J. Hydrol.* **540**, 1136–1145 (2016).
91. Montani, F. & Rosso, O. A. Entropy-complexity characterization of brain development in chickens. *Entropy* **16**, 4677–4692 (2014).
92. Montani, F., Baravalle, R., Montangie, L. & Rosso, O. A. Causal information quantification of prominent dynamical features of biological neurons. *Philos. Trans. R. Soc. A Math. Phys. Eng. Sci.* **373**, 20150109 (2015).
93. Plata, A. et al. Astrocytic atrophy following status epilepticus parallels reduced ca2+ activity and impaired synaptic plasticity in the rat hippocampus. *Front. Mol. Neurosci.* **11**, 215 (2018).
94. Korol, A. M. et al. Preliminary characterization of erythrocytes deformability on the entropy-complexity plane. *Open Med. Informatics J.* **4**, 164 (2010).
95. Siddagangaiah, S. et al. A complexity-based approach for the detection of weak signals in ocean ambient noise. *Entropy* **18**, 101 (2016).
96. Aquino, A. L., Cavalcante, T. S., Almeida, E. S., Frery, A. C. & Rosso, O. A. Characterization of vehicle behavior with information theory. *Eur. Phys. J. B* **88**, 257 (2015).
97. Zunino, L. & Ribeiro, H. V. Discriminating image textures with the multiscale two-dimensional complexity-entropy causality plane. *Chaos Solitons Fractals* **91**, 679–688 (2016).
98. Rosso, O. A., Ospina, R. & Frery, A. C. Classification and verification of handwritten signatures with time causal information theory quantifiers. *PLoS ONE* **11**, e0166868 (2016).
99. Sigaki, H. Y., Perc, M. & Ribeiro, H. V. History of art paintings through the lens of entropy and complexity. *Proc. Natl Acad. Sci. USA* **115**, E8585–E8594 (2018).
100. Olivares, F., Plastino, A. & Rosso, O. A. Contrasting chaos with noise via local versus global information quantifiers. *Phys. Lett. A* **376**, 1577–1583 (2012).
101. Fisher, R. A. In *Mathematical Proc. Cambridge Philosophical Society*, Vol. 22, 700–725 (Cambridge University Press, 1925).
102. Baravalle, R., Rosso, O. A. & Montani, F. Causal Shannon-Fisher characterization of motor/imagery movements in EEG. *Entropy* **20**, 660 (2018).
103. Mateos, D. M., Gomez-Ramirez, J. & Rosso, O. A. Using time causal quantifiers to characterize sleep stages. *Chaos Solitons Fractals* **146**, 110798 (2019).
104. Sippel, S. et al. Diagnosing the dynamics of observed and simulated ecosystem gross primary productivity with time causal information theory quantifiers. *PLoS ONE* **11**, e0164960 (2016).
105. Redelico, F. O., Traversaro, F., Oyarzabal, N., Vilaboa, I. & Rosso, O. A. Evaluation of the status of rotary machines by time causal information theory quantifiers. *Phys. A* **470**, 321–329 (2017).
106. Shang, D. & Shang, P. The Fisher-DisEn plane: a novel approach to distinguish different complex systems. *Commun. Nonlinear Sci. Numerical Simul.* **89**, 105271 (2020).

107. Rostaghi, M. & Azami, H. Dispersion entropy: a measure for time-series analysis. *IEEE Signal Process. Lett.* **23**, 610–614 (2016).
108. Koenig, T., Studer, D., Hubl, D., Melie, L. & Strik, W. Brain connectivity at different time-scales measured with EEG. *Philos. Trans. R. Soc. B Biol. Sci.* **360**, 1015–1024 (2005).
109. Sun, J. et al. Abnormal dynamics of EEG oscillations in schizophrenia patients on multiple time scales. *IEEE Trans. Biomed. Eng.* **61**, 1756–1764 (2014).
110. Mackey, M. C. & Glass, L. Oscillation and chaos in physiological control systems. *Science* **197**, 287–289 (1977).
111. Murayama, S., Kinugawa, H., Tokuda, I. T. & Gotoda, H. Characterization and detection of thermoacoustic combustion oscillations based on statistical complexity and complex-network theory. *Phys. Rev. E* **97**, 022223 (2018).
112. Olivares, F., Zunino, L., Gulich, D., Pérez, D. G. & Rosso, O. A. Multiscale permutation entropy analysis of laser beam wandering in isotropic turbulence. *Phys. Rev. E* **96**, 042207 (2017).
113. Tang, Y., Zhao, A., Ren, Y.-y., Dou, F.-X. & Jin, N.-D. Gas–liquid two-phase flow structure in the multi-scale weighted complexity entropy causality plane. *Phys. A* **449**, 324–335 (2016).
114. Ribeiro, H. V., Jauregui, M., Zunino, L. & Lenzi, E. K. Characterizing time series via complexity–entropy curves. *Phys. Rev. E* **95**, 062106 (2017).
115. Tsallis, C. Possible generalization of Boltzmann–Gibbs statistics. *J. Stat. Phys.* **52**, 479–487 (1988).
116. Argyroudis, G. S. & Siokis, F. M. Spillover effects of great recession on hong-kong’s real estate market: an analysis based on causality plane and Tsallis curves of complexity–entropy. *Phys. A* **524**, 576–586 (2019).
117. Yin, Y., Sun, K. & He, S. Multiscale permutation rényi entropy and its application for EEG signals. *PLoS ONE* **13**, e0202558 (2018).
118. Jauregui, M., Zunino, L., Lenzi, E. K., Mendes, R. S. & Ribeiro, H. V. Characterization of time series via rényi complexity–entropy curves. *Phys. A* **498**, 74–85 (2018).
119. Rényi, A. On measures of information and entropy. In *Proc. 4th Berkeley Symposium on Mathematics, Statistics and Probability* 547–561 (Univ. California Press, 1961).
120. Mao, X., Shang, P., Wang, J. & Ma, Y. Characterizing time series by extended complexity–entropy curves based on Tsallis, Rényi, and power spectral entropy. *Chaos* **28**, 113106 (2018).
121. Tarnopolski, M. On the relationship between the hurst exponent, the ratio of the mean square successive difference to the variance, and the number of turning points. *Phys. A* **461**, 662–673 (2016).
122. Von Neumann, J., Kent, R., Bellinson, H. & Hart, B. T. The mean square successive difference. *Ann. Math. Stat.* **12**, 153–162 (1941).
123. Von Neumann, J. Distribution of the ratio of the mean square successive difference to the variance. *Ann. Math. Stat.* **12**, 367–395 (1941).
124. Zunino, L., Olivares, F., Bariviera, A. F. & Rosso, O. A. A simple and fast representation space for classifying complex time series. *Phys. Lett. A* **381**, 1021–1028 (2017).
125. Żywucka, N., Tarnopolski, M., Böttcher, M., Stawarz, Ł. & Marchenko, V. Optical variability modeling of newly identified blazar candidates behind Magellanic clouds. *Astrophys. J.* **888**, 107 (2020).
126. Toker, D., Sommer, F. T. & D’Esposito, M. A simple method for detecting chaos in nature. *Commun. Biol.* **3**, 1–13 (2020).
127. Theiler, J., Galdrikian, B., Longtin, A., Eubank, S. & Farmer, J. D. Testing for nonlinearity in time series: the method of surrogate data. Technical report. (Los Alamos National Lab., 1991).
128. Jamšek, J., Paluš, M. & Stefanovska, A. Detecting couplings between interacting oscillators with time-varying basic frequencies: instantaneous wavelet bispectrum and information theoretic approach. *Phys. Rev. E* **81**, 036207 (2010).
129. Schreiber, T. Extremely simple nonlinear noise-reduction method. *Phys. Rev. E* **47**, 2401 (1993).
130. Gottwald, G. A. & Melbourne, I. A new test for chaos in deterministic systems. *Proc. R. Soc. Lond. Ser. A Math. Phys. Eng. Sci.* **460**, 603–611 (2004).
131. Gottwald, G. A. & Melbourne, I. Testing for chaos in deterministic systems with noise. *Phys. D* **212**, 100–110 (2005).
132. May, R. M. Simple mathematical models with very complicated dynamics. *Nature* **261**, 459–467 (1976).
133. Sprott, J. C. *Chaos and Time-Series Analysis* (Oxford University Press, 2003).
134. Rosso, O. A. et al. Characterization of chaotic maps using the permutation Bandt–Pompe probability distribution. *Eur. Phys. J. B* **86**, 116 (2013).
135. Kulp, C. W., Zunino, L., Osborne, T. & Zawadzki, B. Using missing ordinal patterns to detect nonlinearity in time series data. *Phys. Rev. E* **96**, 022218 (2017).
136. Piek, A. B., Stolz, I. & Keller, K. Algorithmics, possibilities and limits of ordinal pattern based entropies. *Entropy* **21**, 547 (2019).

Acknowledgements

This project has received funding from the European Research Council (ERC) under the European Union’s Horizon 2020 research and innovation programme (grant agreement No. 851255). Financial support has been received from the Agencia Estatal de Investigación (AEI, MCI, Spain) and Fondo Europeo de Desarrollo Regional (FEDER, UE), under the María de Maeztu Program for units of Excellence in R&D (MDM-2017-0711).

Competing interests

The authors declare no competing interests.

Additional information

Supplementary information The online version contains supplementary material available at <https://doi.org/10.1038/s42005-021-00696-z>.

Correspondence and requests for materials should be addressed to M.Z.

Peer review information *Communications Physics* thanks the anonymous reviewers for their contribution to the peer review of this work. Peer reviewer reports are available.

Reprints and permission information is available at <http://www.nature.com/reprints>

Publisher’s note Springer Nature remains neutral with regard to jurisdictional claims in published maps and institutional affiliations.



Open Access This article is licensed under a Creative Commons Attribution 4.0 International License, which permits use, sharing, adaptation, distribution and reproduction in any medium or format, as long as you give appropriate credit to the original author(s) and the source, provide a link to the Creative Commons license, and indicate if changes were made. The images or other third party material in this article are included in the article’s Creative Commons license, unless indicated otherwise in a credit line to the material. If material is not included in the article’s Creative Commons license and your intended use is not permitted by statutory regulation or exceeds the permitted use, you will need to obtain permission directly from the copyright holder. To view a copy of this license, visit <http://creativecommons.org/licenses/by/4.0/>.

© The Author(s) 2021